Korean J. Chem. Eng., 36(5), 816-821 (2019)
DOI: 10.1007/s11814-019-0264-4

pISSN: 0256-1115
eISSN: 1975-7220

An efficient near-infrared-responsive photocatalyst of flower-like Gd^{3+}-doped WS_2

Woocheol Kim and Younghun Kim†

Department of Chemical Engineering, Kwangwoon University, 20 Kwangwoon-ro, Nowon-gu, Seoul 01897, Korea
(*Received 16 February 2019 • accepted 1 April 2019*)

Abstract−To improve the utilization efficiency of sunlight, near-infrared (NIR)-responsive Gd^{3+}-doped WS_2 was prepared by a microwave-assisted solvothermal method. The microwave-assisted method required 1 h to synthesize the particles. To examine the activity of the photocatalyst under only NIR laser irradiation, its photocatalytic activities were evaluated by monitoring the degradation of Rhodamine B under 808 nm NIR laser irradiation. The NIR-responsive photocatalyst can also be used in the UV and visible light regions having shorter wavelengths than the NIR region. Photoactivity under a broader range of wavelengths can lead to more efficient photocatalytic reactions. Since NIR radiation has high permeability, the IR-photocatalytic reaction can be successfully carried out even on cloudy days or in damp environments. To prove this, the NIR laser was passed through a milk layer, following which a photocatalytic reaction experiment was conducted.

Keywords: Photocatalyst, WS_2, Near-infrared Laser, Degradation of Rhodamine B

INTRODUCTION

Semiconductor photocatalysis has been studied in various fields, including water purification, the production of hydrogen, and the elimination of toxic substances. For these applications, solar energy and green chemistry have diverse advantages of clean and safe energy production with no release of other undesirable chemicals as well as reusability [1-3]. TiO_2 is a representative photocatalyst because of its low cost, stability, and abundance. Despite these advantages, TiO_2 exhibits decreased photoactivity under visible light compared to UV irradiation [4]. Therefore, photocatalysts activated by light of longer wavelengths have the potential to be reactive under light of shorter wavelengths because the light of shorter wavelength has higher energy.

A few studies have been performed to synthesize near-infrared (NIR)-responsive photocatalysts with Ag_2O, Ag_2S, and amorphous TiO_2 [5-12]. The most important feature as NIR-driven photocatalysts is the extension of absorption range of the compound into infrared region, thus remarkably increasing the utilization rate of solar energy [9]. That is, the formation of a middle energy level between the valence band and conduction band enables the energy of NIR light to be transferred to the conduction band of a semiconductor material. The doping of metal ions into the lattice of semiconductor materials is usually utilized to increase the photocatalytic efficiency by preventing the photoexcited electrons and holes from being recombined. On the other hand, doping of other materials could play a role in overcoming the broad band gap for the absorption of NIR light. The photoexcited electrons can then reach the conduction band by stepping through several energy levels [13-16].

In this work, brown tungsten disulfide (WS_2) was selected as the semiconductor because of its strong absorbance in the NIR region [17]. WS_2 has a higher absorbance in the NIR wavelength range than other photocatalysts, such as TiO_2, CdS, and SnS_2. Because WS_2 can absorb enough light in the NIR region, it has a greater possibility to react under NIR irradiation. Research has been published describing photothermal therapy (PTT) by doping ions into the lattice of WS_2 [17]. In this paper, we considered several metal ions (Fe^{3+}, Co^{2+}, Ni^{2+}, Mn^{2+}, Gd^{3+}) for preparing $WS_2 : M^{n+}$ with different metal doping levels using a high-temperature solution method by reacting WCl_6 and MCl_x. Similarly, in our study, Gd^{3+} was selected as the best dopant for WS_2 to make an NIR-responsive photocatalyst by using a microwave-assisted method. The photocatalytic ability of Gd^{3+}-doped WS_2 was then evaluated through the degradation of Rhodamine B dye under 808 nm laser irradiation.

EXPERIMENTAL

1. Synthesis of Gd^{3+}-doped WS_2

All reagents purchased from Sigma-Aldrich were of analytical grade and used as-received without further purification. In the typical synthetic process for Gd^{3+}-doped WS_2, 10 mM or 20 mM (5 or 10 atomic percent) gadolinium(III) chloride hexahydrate ($GdCl_6 \cdot 6H_2O$), 0.1 M thioacetamide (TAA, CH_3CSNH_2) and 62.5 mM tungsten(VI) chloride (WCl_6) were dissolved in 40 mL anhydrous ethanol with magnetic stirring for 1 h. For the synthesis of WS_2, the same synthesis process was carried out without $GdCl_6 \cdot 6H_2O$. The resulting solution was transferred into a 100-mL Teflon vessel, followed by microwave-heating (100 °C for 1 h) in a microwave reaction system (MARS6, CEM) at 1.8 kW and a magnetron frequency of 2.46 GHz. After heating, the Teflon vessel was cooled to room temperature and sonicated for 5 min to detach any particles on the walls of the vessel. The obtained dark brown colored particles were washed with anhydrous ethanol several times to remove any residue. Finally, the particles were dried at 80 °C in an oven for

†To whom correspondence should be addressed.
E-mail: korea1@kw.ac.kr

a day. As a result, pure WS_2 and 5% and 10% Gd^{3+}-doped WS_2 were synthesized by a microwave-heating method for photocatalytic testing under an 808 nm NIR laser.

2. Photocatalytic Degradation of Rhodamine B

For the photocatalytic activity tests under NIR laser (<4 W/cm^2) irradiation, an organic dye, Rhodamine B, was used as the substance to be degraded. An NIR laser was used as the NIR source (λ=808 nm). Photocatalytic degradation tests were performed with 20 to 40 mg of photocatalyst. Photocatalyst was added to Rhodamine B aqueous solutions (80 mL, 20 mg/L) with 1.02 mM formic acid (HCOOH) as a hole scavenger. The solution was transferred to a vial in the dark to prevent exposure to any external light. To ensure enough adsorption of Rhodamine B, the solution was stirred in the dark for 24 h and then irradiated with the NIR laser from top to bottom. Due to the low power of the NIR laser, 1 mL of the suspension was extracted at 3 h intervals to ensure enough energy transfer. After centrifuging the suspension to analyze the concentration of the supernatant, the degradation results were determined by measuring the absorbance at a wavelength of 521 nm using a UV-vis spectrometer (UV-1800, Shimadzu). Moreover, for permeability tests of the 808 nm NIR laser, white milk was placed between the solution and the laser. A permeability experiment with a milk layer was also performed with the same experimental conditions.

3. Characterization

The crystalline structure and morphology of the as-made Gd^{3+}-doped WS_2 particles were examined by X-ray diffraction (XRD; Bruker, DE/D8 Advance), high-resolution field effect scanning electron microscopy (HR-FE-SEM; SU8010, HITACHI), and transmission electron microscopy (TEM; JEM-2010, JEOL). The absorbance spectra and band gap energy data were analyzed by UV-vis diffuse reflectance spectroscopy (DRS; V-670, JASCO). Photoluminescence spectroscopy (PL, Perkin Elmer, LS55) was performed to analyze the intensity of light produced by photoexcited electrons.

Fig. 1. Schematic of formation mechanism of Gd^{3+}-doped WS_2 particles.

RESULTS AND DISCUSSION

1. Characterization

Gd^{3+}-doped WS_2 was synthesized by a microwave-assisted method according to the formation mechanism (Fig. 1). Microwave methodologies are suitable to synthesize nanostructure WS_2 under mild conditions with a short reaction time and low temperature, compared to conventional hydrothermal method. Several nanoparticles were assembled and grown to rod shape. Then, the rod-like particles were grown to dandelion-like photocatalyst particles. After the microwave-assisted reaction, brown colored photocatalyst was obtained. The morphology for the dandelion-like structure of the Gd^{3+}-doped WS_2 particles was confirmed by using HR-FE-SEM (Fig. 2). Although the ratio of Gd^{3+} in the lattice of WS_2 was different, each sample exhibited similar morphology. The doping of Gd^{3+} ions was not influencing the morphological change of parent WS_2 material. The corresponding elemental mapping was conducted to investigate the distribution of elements in the Gd^{3+}-doped WS_2. As shown SEM-EDS (Fig. 3), S, Gd, and W elements are distributed evenly in the particles. Through TEM-EDS analysis, the proportion of components (Gd, W, S) was analyzed (Fig. 4). According to the ratio of components, the ratio of 10% and 5% Gd^{3+}-doped WS_2 samples was actually 10.7 and 3.3 atomic %, respectively.

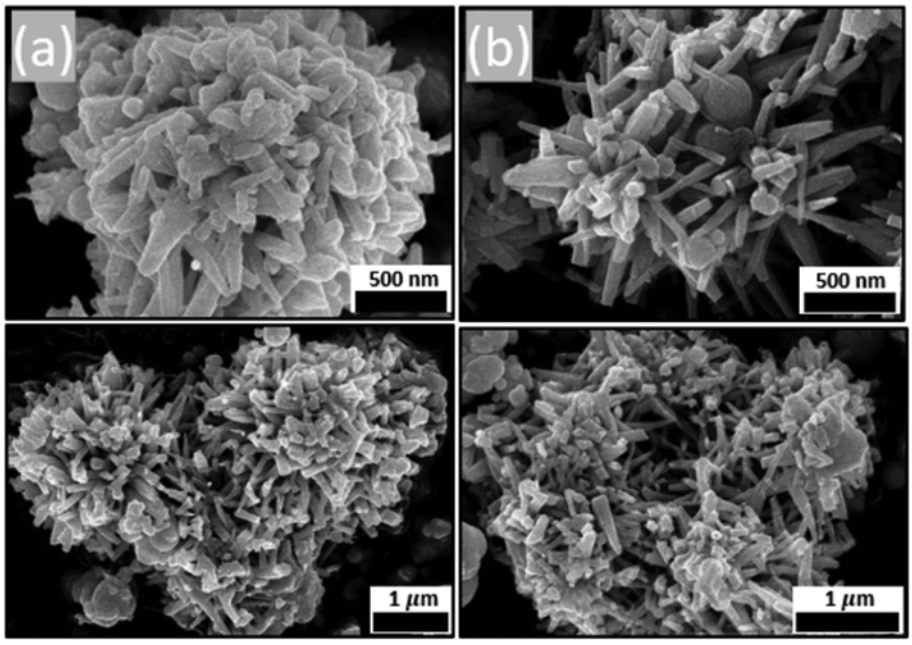

Fig. 2. HR-FE-SEM images of (a) 10% and (b) 5% Gd^{3+}-doped WS_2 particles.

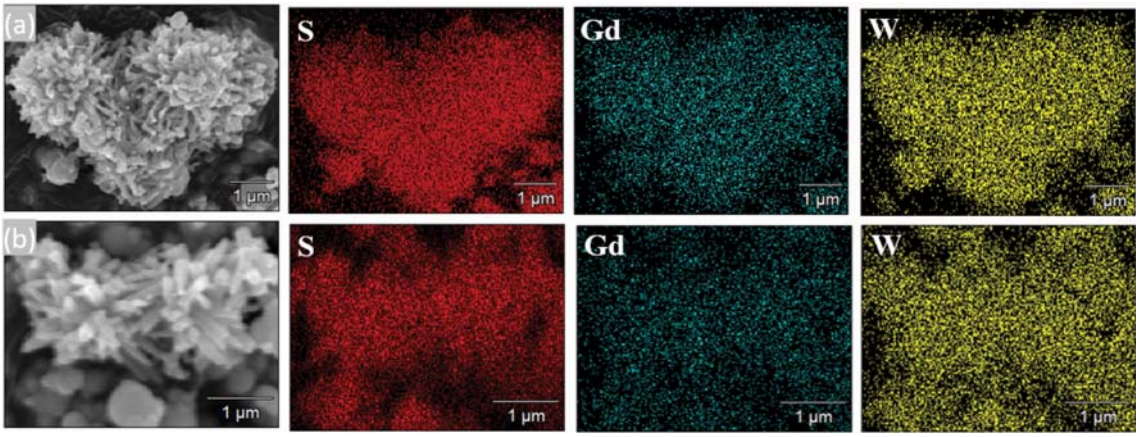

Fig. 3. EDS mapping image of (a) 10% and (b) 5% Gd^{3+}-doped WS_2.

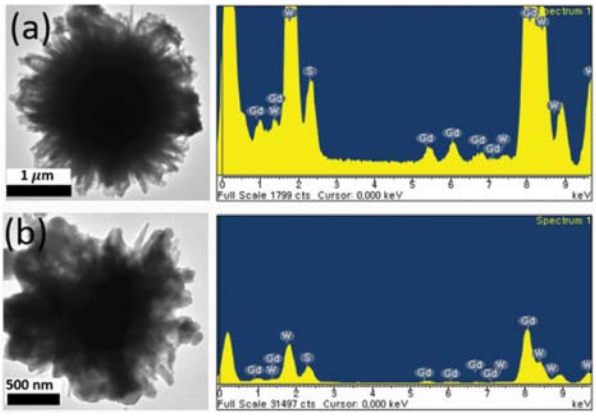

Elemental	at %
Gd	10.67
W	47.06
S	42.27

Elemental	at %
Gd	3.29
W	34.20
S	65.52

Fig. 4. TEM images and EDS profiles of (a) 10% and (b) 5% Gd^{3+}-doped WS_2.

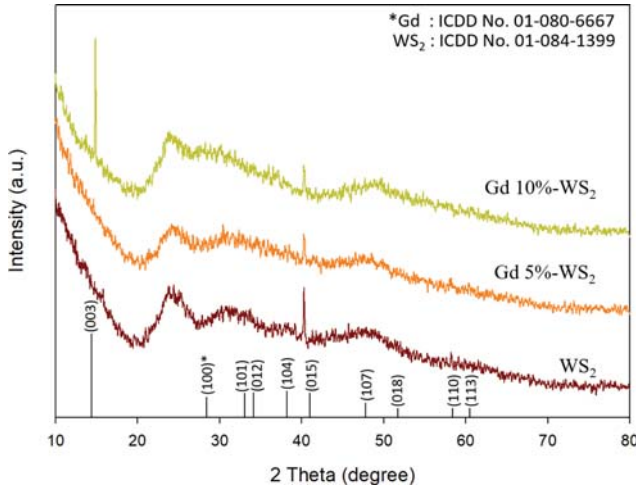

Fig. 5. XRD patterns of pure WS_2 and 10% and 5% Gd^{3+}-doped WS_2 particles.

The crystallinity of the samples was compared according to the ratio of Gd^{3+} (Fig. 5). A similar pattern to those of Gd^{3+}-doped WS_2 was found for pure WS_2. It is noted that the crystallinity of the samples was not changed with small content of doping with Gd^{3+}. As increasing of Gd^{3+} doping in WS_2, the shoulder peak at 28° for (100) plane of Gd was slightly increased. To investigate the photoexcitation in the NIR region, PL intensities induced by 325 nm excitation were confirmed at wavelengths around 500 and 800 nm (Fig. 6). The photoactivity of Gd^{3+}-doped WS_2 in the NIR region was confirmed from the intensity response. Comparing the two doping ratios, 5% Gd^{3+}-doped WS_2 exhibited a higher intensity in both the visible light (500 nm) and NIR (800 nm) regions. The higher intensities mean more electrons were photoexcited by visible and NIR light. In addition, as shown in the UV-vis DRS spectrum (Fig. 7), the absorbance in the NIR region was high enough for the sample to act as photocatalyst. The 5% Gd^{3+}-doped WS_2 sample had higher absorbance in the 400-1,000 nm wavelength range. More absorption of light in the NIR region could result in higher efficiency (Fig. 7(a)). The band gap energy (E_g) of the semiconductor could be calculated using Tauc's formula and the graph shown in Fig. 7(b):

$$(\alpha h\nu)^2 = A(h\nu - E_g)^n$$

Fig. 7(b) shows the band gaps calculated from the onset of the absorption edge, which are 1.51 eV and 1.59 eV for 5% and 10% Gd^{3+}-doped WS_2, respectively. The band gaps were narrow enough to allow reaction under irradiation by an 808 nm NIR laser [8]. Even though the difference in the band gap was small, it still resulted

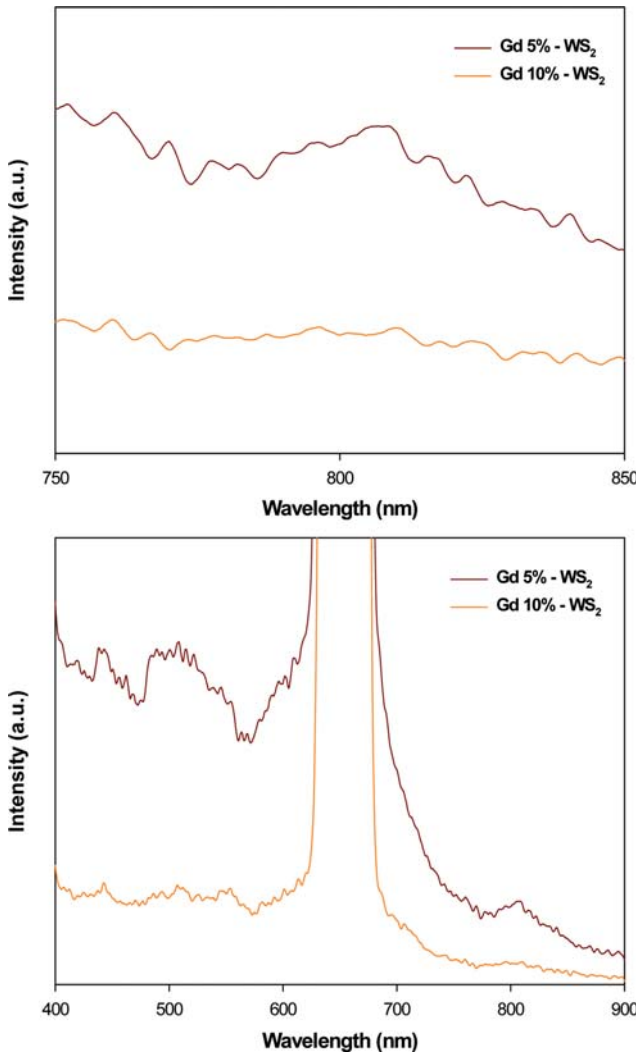

Fig. 6. Photoluminescence spectra of 10% and 5% Gd^{3+}-doped WS_2.

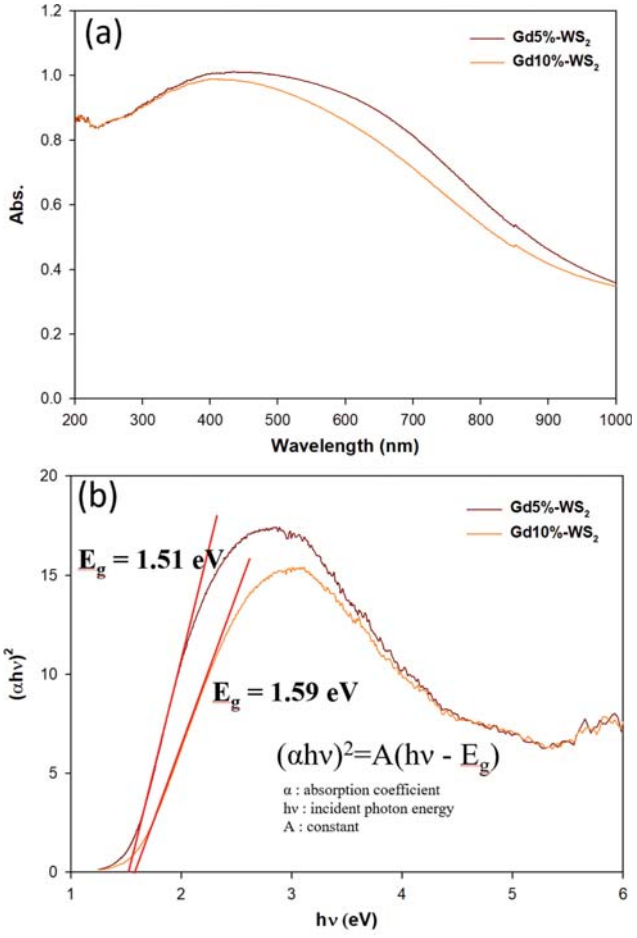

Fig. 7. (a) UV-vis DRS spectrum and (b) band gap energy estimated by plotting $(\alpha h\nu)^{1/2}$ versus the photo energy ($h\nu$) of Gd^{3+}-doped WS_2.

in enhanced photocatalytic performance.

2. Photocatalytic Activity of Gd^{3+}-doped WS_2

The separation of electron and hole pairs can progress easily under irradiation with UV or visible light of sufficient energy. However, an NIR laser that has lower energy cannot always excite electrons from the valence to the conduction band. The photoexcited electrons that do not reach the conduction band are readily recombined with holes. To facilitate the separation of electrons and holes, another energy level was formed between the valence band and conduction band by the impurity dopant [13-17]. As shown in Fig. 8, which depicts the mechanism of the reaction, electrons are excited to the energy level of Gd^{3+} by NIR laser irradiation. The doping of Gd^{3+} on the WS_2 might be forming a middle energy level between the valence band and conduction band. This energy level plays the role of a bridge that can connect the upper band and lower band. Then, the electrons at the energy level of Gd^{3+} are transferred to the conduction band by the continuous irradiation of NIR energy. Thus, the photoexcited electrons combine with oxygen molecules (O_2), and super oxide ($\cdot O_2^-$) is formed. Simultaneously, the generated holes combine with hydroxide (OH^-), and hydroxyl radicals

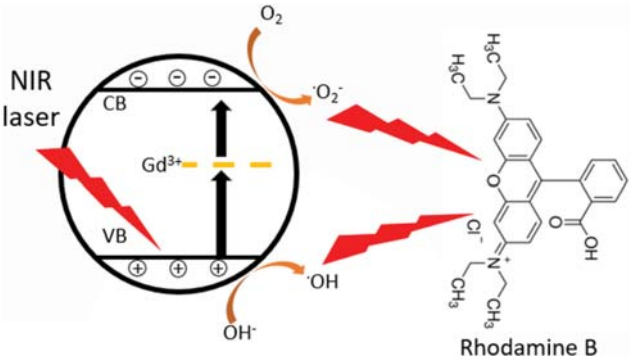

Fig. 8. Schematic diagram of a possible photocatalytic Rhodamine B degradation mechanism by Gd^{3+}-doped WS_2 under 808 nm NIR laser irradiation.

($\cdot OH^-$) are formed. The OH^- and $\cdot OH^-$ molecules, which are strong oxidizing agents, are then used to degrade the Rhodamine B dye.

In the degradation experiments using Rhodamine B, the three samples were investigated for their efficiency. Before irradiation with the NIR laser, the dark adsorption of the photocatalysts was measured using organic dye. The characteristic peak of Rhodamine B is

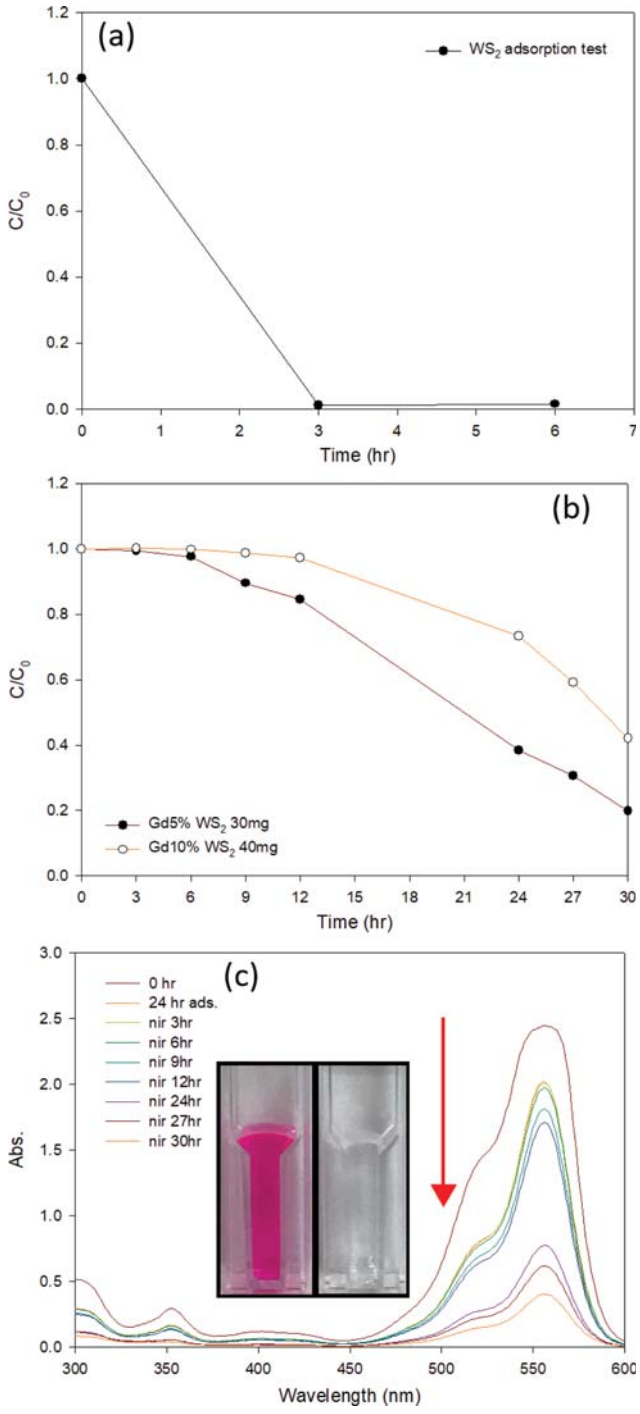

Fig. 9. (a) Dark adsorption test with 20 mg WS_2, (b) variation of normalized (C/C_0) concentration in the presence of 10% and 5% Gd^{3+}-doped WS_2 and (c) time dependent UV-vis absorption spectrum of RhB (C_0=20 mg/L) with irradiation time under 808 nm NIR laser exposure in the presence of 5% Gd^{3+}-doped WS_2 particles.

at 521 nm, which was dramatically reduced after 3 h of exposure due to adsorption by 20 mg of WS_2 without Gd^{3+} (Fig. 9(a)). Because of the significant adsorption of Rhodamine B by WS_2, its degradation could not be evaluated under NIR irradiation. It means that WS_2 without Gd^{3+} doping was not suitable to apply NIR-responsive photocatalyst due to their high adsorption rate for organic dye. The 5% and 10% Gd^{3+}-doped WS_2 samples were investigated after adsorption for 24 h (Fig. 9(b)). As results in the PL spectra and the absorbance and band gap calculated by UV-vis DRS analysis, 5% Gd^{3+}-doped WS_2 has more efficient photoactivity under 808 nm laser irradiation. Through the Rhodamine B degradation experiment, the degradation rate with 30 mg of 5% Gd^{3+}-doped WS_2 was found to be faster than that with 40 mg of 10% Gd^{3+}-doped WS_2. Fig. 9(c) shows the time-dependence of the photocatalytic degradation of Rhodamine B under 808 nm NIR laser irradiation in the presence of 5% Gd^{3+}-doped WS_2. After complete degradation, the dark pink color of Rhodamine B faded, leaving a transparent solution. Then, to perform a permeability test of the 808 nm NIR laser, a 2-cm thick white milk layer was placed between the NIR laser and the solution with 30 mg of 5% Gd^{3+}-doped WS_2 (Fig. 10). The efficiency decreased compared to when there was no milk layer. The intensity of the laser was weakened as it passed through the milk. However, the permeability test of the NIR demonstrates that the NIR-responsive photocatalyst can be used on cloudy days or in damp places.

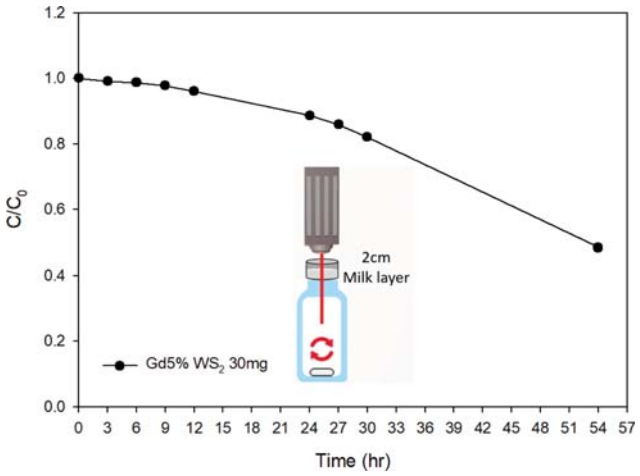

Fig. 10. Milk layer permeability test of 808 nm NIR laser in the presence of 5% Gd^{3+}-doped WS_2.

CONCLUSIONS

Most photocatalyst studies have been conducted using UV or visible light-responsive photocatalysts. However, the NIR region constitutes about half of the sun's light. Therefore, an NIR-responsive photocatalyst can take advantage of a larger spectrum of light. Gd^{3+}-doped WS_2 was easily synthesized by a microwave method. The absorbance as a function of wavelength and band gap were measured through UV-vis DRS spectrometry. The 5% Gd^{3+}-doped WS_2 sample had higher absorbance in the visible light and NIR regions and a narrower band gap than the 10% Gd^{3+}-doped WS_2 sample. The photocatalytic efficiency of the samples was evaluated through Rhodamine B degradation experiments in an aqueous medium. 5% Gd^{3+}-doped WS_2 with 30 mg showed 84% degradation efficiency of dye, compared to 10% Gd^{3+}-doped WS_2 with 40 mg. In addition, the results of permeability tests of the NIR laser

demonstrated that the NIR-responsive photocatalyst can be used on cloudy days or in damp places.

ACKNOWLEDGEMENTS

This work was conducted during the sabbatical year of Kwangwoon University in 2019 with research fund of the National Research Foundation of Korea (NRF-2017R1A2B4001829).

REFERENCES

1. J. Yu, S. Zhuang, X. Xu, W. Zhu, B. Feng and J. Hu, *J. Mater. Chem. A*, **3**, 1199 (2015).
2. T. Su, Q. Shao, Z. Qin, Z. Guo and Z. Wu, *ACS Catal.*, **8**, 2253 (2018).
3. T. Su, R. Peng, Z. D. Hood, M. Naguib, I. N. Ivanov, J. K. Keum, Z. Qin, Z. Guo and Z. Wu, *Chemsuschem*, **11**, 688 (2018).
4. N. N. Bahrudin and M. A. Nawi, *Korean J. Chem. Eng.*, **36**, 478 (2019).
5. W. Jiang, X. Wang, Z. Wu, X, Yue, S. Yuan, H. Lu and B. Liang, *Ind. Eng. Chem. Res.*, **54**, 832 (2015).
6. W. Jiang, Z. Wu, X. Yue, S. Yuan, H. Lu and B. Liang, *RSC Adv.*, **5**, 24064 (2015).
7. A. Gannoruwa, B. Ariyasinghe and J. Bandara, *Catal. Sci. Technol.*, **6**, 479 (2016).
8. J. Jiang, X. Tang, S. Zhou, J. Ding, H. Zhou, F. Zhang, D. Di and T. Fan, *Green Chem.*, **18**, 2056 (2016).
9. Z. Zhang and W. Wenzhong, *Dalton Trans*, **42**, 12072 (2013).
10. H. Li, R. Liu, Y. Liu, H. Huang, H. Yu, H. Ming, S. Lian, S.-T. Lee and Z. Kang, *Mater. Chem.*, **22**, 17470 (2012).
11. J. Chen, H. Che, K. Huang, C. Liu and W. Shi, *Appl. Catal. B: Environ.*, **192**, 134 (2016).
12. W. Qin, D. Zhang, D. Zhao, W. Lili and K. Zheng, *Chem. Commun.*, **46**, 2304 (2010).
13. X. Guo, W. Di, C. Chen, C. Liu, X. Wang and W. Qin, *Dalton Trans.*, **43**, 1048 (2014).
14. W. Wang, W. Huang, Y. Ni, C. Lu and Z. Xu, *ACS Appl. Mater. Interfaces*, **6**, 340 (2013).
15. Y. Tang, W. Di, X. Zhai, R. Yang and W. Qin, *ACS Catal.*, **3**, 405 (2013).
16. X. Guo, W. Song, C. Chen, W. Di and W. Qin, *Phys. Chem. Chem. Phys.*, **15**, 14681 (2013).
17. L. Cheng, C. Yuan, S. Shen, X. Yi, H. Gong, K. Yang and Z. Liu, *ACS Nano*, **9**, 11090 (2015).